Heat Transfer

WILEY

HEAT TRANSFER

ORIGINAL ARTICLE

Thermal and Entropic Analysis of Viscous Fluid Flow in a Porous Channel With Convective Heat Transfer and Magnetic Field Aspects

Odeli J. Kigodi[1] | Nyanga H. Masasila[2,3] | Muhammad Faisal[4,5] | Irfan Anjum Badruddin[6] | Ahmed Said Abdel Hafez Zedan[6] | Chacha S. Chacha[7]

[1]Department of Engineering, Mtwara Campus-College of Technical Education, Mbeya University of Science and Technology, Mtwara, Tanzania | [2]Department of General Studies, Dar es salaam Institute of Technology, Dar es Salaam, Tanzania | [3]Doctoral School of Informatics, University of Debrecen, Debrecen, Hungary | [4]Department of Mathematics, Faculty of Science, The University of Azad Jammu and Kashmir, King Abdullah Campus, Muzaffarabad, Pakistan | [5]Applied Science Research Center, Applied science Private University, Amman, Jordan | [6]Mechnical Engineering Department, College of Engineering, King Khalid University, Abha, Saudi Arabia | [7]Department of Mathematics, Physics, and Informatics, Mkwawa University College of Education, University of Dar es Salaam, Iringa, Tanzania

Correspondence: Muhammad Faisal (faisalmzd225@gmail.com)

Received: 7 October 2025 | **Revised:** 15 December 2025 | **Accepted:** 27 December 2025

Funding: Deanship of Research and Graduate Studies at King Khalid University, Grant/Award Number: RGP.2/246/46

Keywords: convective heat transfer | entropy | magnetic field | porous channel | viscous fluid flow

ABSTRACT

This study examines the thermal and entropy generation characteristics of viscous fluid flow through a porous channel under convective cooling and magnetic field effects. The flow is modeled using the steady state momentum and energy equations and solved numerically via a finite difference scheme. Parametric variations in Darcy number (Da), magnetic parameter (M), pressure gradient (A), Biot number (Bi), Prandtl number (Pr), Eckert number (Ec), and internal heat generation (Q) are analyzed. Results show that increasing M from 0 to 20 reduces entropy generation by approximately 18%, while raising Bi from 0 to 0.6 decreases entropy by about 12%. Higher Da and Q promote thermal buildup but increase irreversibility, whereas stronger M and Bi stabilize flow, lower temperatures, and improve thermodynamic efficiency. The Nusselt number increases with Bi and Ec, enhancing heat transfer, while skin friction decreases with stronger magnetic fields. These findings provide practical guidance for selecting permeability, magnetic field strength, and surface heat transfer characteristics to optimize energy efficiency and thermal performance in porous channel thermal systems and magnetohydrodynamic applications.

1 | Introduction

The thermal and entropic study of viscous fluid motion in channels with porous structures considering heat transfer by convection and magnetic field aspects is crucial due to its relevance in diverse applications such as biomedical flows, chemical processing, geothermal energy systems, and various engineering technologies. Investigating heat and momentum transport under the influence of wall suction or injection, along with convective thermal conditions, is vital for enhancing system efficiency and reducing energy losses [1–4]. Studies such as those by Makinde [5, 6], Kigodi et al. [7], Mkwizu [8], Kigodi and Honda [9] have demonstrated that entropy analysis provides deeper insight into the performance of heat transfer systems, especially in magneto-hydrodynamic (MHD) and convective flow regimes.

Much research has been conducted on various fluid types-including Newtonian, non-Newtonian, nanofluids, and hybrid nanofluids-in porous media or between permeable or stretching surfaces. For instance, Makinde and collaborators extensively

investigated entropy generation in MHD flows, incorporating effects such as thermal radiation, viscous dissipation, and chemical reactions [3, 10, 11]. Likewise, Mahmud and Fraser [4], and Chamkha and Sheikholeslami [12] examined irreversibility phenomena in thermally driven flows through porous geometries and under forced convection conditions. Faisal et al., also contributed significantly to this field through studies on MHD flows with various energy transport mechanisms [13–15].

Additional investigations by Khan et al. [16], Sindhu and Gireesha [17] addressed entropy generation under various thermal and magnetic field configurations. Similarly, Nandeppanavar et al. [18], Sheikholeslami et al. [19], and Murugan et al. [20] explored entropy optimization in nanofluid and porous systems. Other related studies include those by Kameswaran et al. [21], Mohamed et al. [22], and Mejri et al. [23].

Recent advancements have expanded the scope to more complex systems. Mahian et al. [24], Makinde and Aziz [25], and Rashidi et al. [26] investigated the impact of nanofluids, porous geometries, and rotating disks on entropy generation. Ahmad et al. [27], Biswas et al. [28], Mkwizu et al. [29], and Mfinanga and Iddi [30] further emphasized the role of entropy-based optimization under magnetic and hybrid nanofluid influences.

Additionally, Mandal et al. [31], Rauf et al. [32], and Sakkaravarthi et al. [33] extended this analysis to emerging flow systems. Kiamari et al. [34], Abuasbeh et al. [35], and Abbas et al. [36] also contributed valuable inputs into entropy generation in peristaltic flows and non-Newtonian hybrid nanofluids.

More interestingly, various studies emphasize the inclusion of non-Newtonian rheology, magnetic field effects, radiation, and convective boundary conditions for improved physical realism. Subrahmanyam et al. [37] and Fazuruddin et al. [38] investigated MHD nanofluid and micropolar flows incorporating convective cooling, radiation, Lorentz force, and activation energy effects. Furthermore, advanced numerical investigations using finite volume, finite difference, and lattice Boltzmann methods have clarified the influence of Joule heating, buoyancy, and non-Darcy porous effects in magnetized enclosures [39–41]. Additionally, hybrid nanofluid and Casson fluid convection studies in complex porous cavities revealed the critical roles of magnetic field intensity and radiation on heat transfer and entropy generation [42, 43]. Collectively, these works motivate the development of comprehensive MHD models incorporating unsteady behavior, porous resistance, convective cooling, and thermodynamic irreversibility. In this work, a revised mathematical framework is proposed to examine the steady and incompressible MHD flow of a viscous fluid within a porous channel, subject to uniform wall suction or injection and convective thermal conditions. The analysis accounts for key physical influences such as magnetic field intensity, resistance imposed by the porous matrix, internal thermal energy generation, and heat exchange at the boundaries. Distinct from previous approaches, this model integrates the concept of entropy generation to quantify the degree of irreversibility arising from both viscous and thermal dissipation mechanisms, thereby providing a more detailed insight into the thermodynamic behavior of such complex flow systems.

Also, the study aims to address the following research questions: How do magnetic field strength, porous resistance, and internal heat generation affect velocity, temperature, and entropy generation profiles? What is the influence of convective boundary conditions on thermal irreversibility? How do variations in key dimensionless parameters impact the overall flow and heat transfer characteristics? To what extent do these parameters alter the values of thermal and frictional boundary characteristics? and How can entropy analysis guide energy-efficient system design under such multi-physical interactions? (Figure 1).

2 | Formulation of the Model

We consider a steady, incompressible, and electrically conducting viscous fluid flow between two stationary parallel plates embedded in a porous medium. The flow is driven by a constant pressure gradient along the x-direction, while a uniform magnetic field is applied perpendicular to the flow direction. The lower plate is maintained at a prescribed non-uniform temperature, whereas the upper plate dissipates heat to the surrounding environment via convective cooling. Additionally, internal heat generation within the fluid is taken into account. The governing Equations (1), (2), and (10) in the present study are extensions and adaptations of the mathematical formulations developed by Makinde and Eegunjobi [44], who investigated entropy generation in channel flow with convective heating and permeable walls. Their model establishes a base structure upon which additional physical aspects related to heat and entropy can be incorporated. The formulation of the model is based on the following assumptions:

- The fluid is Newtonian and incompressible.
- All thermo-physical properties of the fluid are constant.
- The flow is one-dimensional, with velocity varying only in the transverse direction.

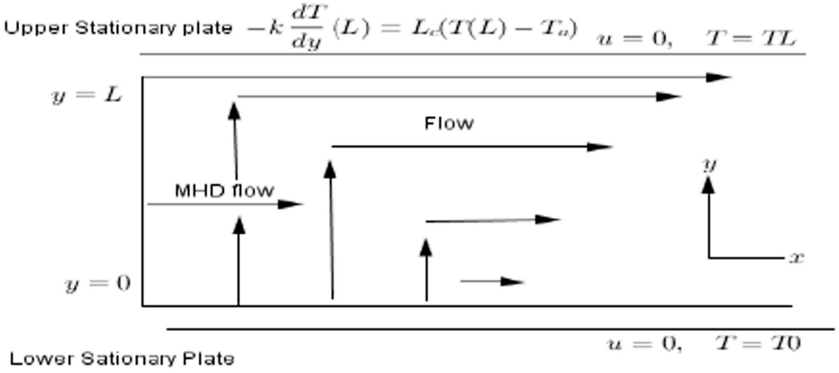

FIGURE 1 | Schematic flow diagram for thermal and entropic.

- The magnetic Reynolds number is sufficiently small, so that the induced magnetic field is negligible compared to the applied magnetic field.
- Hall and ion-slip effects are neglected.
- The porous medium is isotropic, homogeneous, and fully saturated.
- Viscous dissipation and internal heat generation within the fluid are taken into account.
- Thermal radiation effects are neglected.
- At the upper plate ($y = L$), heat is transferred from the plate to an ambient air cooling at a constant temperature T_a. The corresponding convective boundary condition is given by

$$-k\frac{dT}{dy}(L) = L_c(T(L) - T_a),$$

which follows Newton's law of cooling, where L_c is the convective heat transfer coefficient.

The one-dimensional steady-state governing equations for momentum and energy in the y-direction are given by

$$\frac{du}{dx} = 0, \tag{1}$$

$$\nu\frac{d^2u}{dy^2} - \left(\frac{\mu}{K} + \frac{\sigma B_0^2}{\rho}\right)u = \frac{1}{\rho}\frac{dP}{dx}, \tag{2}$$

$$\alpha\frac{d^2T}{dy^2} + \frac{\mu}{\rho c_p}\left(\frac{du}{dy}\right)^2 + \frac{\sigma B_0^2 u^2}{\rho c_p} + \frac{Q_0}{\rho c_p} = 0. \tag{3}$$

Let L be the distance between the plates. The BCs are

$$u(0) = 0,\ T(0) = T_w, \tag{4}$$

$$u(L) = 0,\ -k\frac{dT}{dy}(L) = L_c(T(L) - T_a). \tag{5}$$

We introduce the following dimensionless quantities:

$$\begin{aligned} &\xi = \frac{y}{L},\ W = \frac{u}{U_0},\ \theta = \frac{T - T_a}{T_w - T_a},\ A = \frac{1}{\nu U_0}\frac{dP}{dx},\\ &Pr = \frac{\nu}{\alpha},\ Ec = \frac{U_0^2}{c_p(T_w - T_a)},\ M = \frac{\sigma B_0^2 L^2}{\rho\nu},\ Da = \frac{K}{L^2},\\ &Q = \frac{Q_0 L^2}{k(T_w - T_a)},\ Bi = \frac{L_c L}{k}. \end{aligned} \tag{6}$$

The momentum equation results to:

$$\frac{d^2W}{d\xi^2} - \left(\frac{1}{Da} + M\right)W = \frac{1}{\nu U_0}\frac{dP}{dx}. \tag{7}$$

Eliminating the pressure gradient in the dimensionless momentum equation: the RHS stands for pressure gradient along the x-direction. The pressure gradient $\frac{dP}{dx}$ is assumed to be constant, it acts as a constant source term. Let us define

$$A = \frac{1}{\nu U_0}\frac{dP}{dx},$$

which yields the simplified form of the momentum equation:

$$\frac{d^2W}{d\xi^2} - \left(\frac{1}{Da} + M\right)W = A. \tag{8}$$

and the simplified energy equation is:

$$\frac{1}{\mathrm{Pr}}\frac{d^2\theta}{d\xi^2} + \mathrm{Ec}\left(\frac{dW}{d\xi}\right)^2 + \mathrm{EcMW}^2 + Q = 0, \tag{9}$$

with BC

$$W_0 = 0,\ \theta_0 = 1, \tag{10}$$

$$W_1 = 0,\ \frac{d\theta}{d\xi}(1) = -\mathrm{Bi}\ \theta_1. \tag{11}$$

The dimensional form of the local volumetric entropy production rate E_P is:

$$E_P = \frac{k}{T^2}\left(\frac{dT}{dy}\right)^2 + \frac{\mu}{T}\left(\frac{du}{dy}\right)^2 + \frac{\sigma B_0^2 u^2}{T}. \tag{12}$$

In dimensionless form, the entropy production number N_s is given by:

$$N_s = \frac{1}{\theta^2}\left(\frac{d\theta}{d\xi}\right)^2 + Br\left[\left(\frac{dW}{\partial\xi}\right)^2 + \mathrm{MW}^2\right], \tag{13}$$

where

$$\mathrm{Br} = \frac{\mu U_0^2}{k(T_w - T_a)}.$$

Bejan Number: The dimensionless entropy generation number can be decomposed into thermal and fluid friction irreversibility components as

$$N_s = N_{s,h} + N_{s,f},$$

where

$$N_{s,h} = \frac{1}{\theta^2}\left(\frac{d\theta}{d\xi}\right)^2,$$

represents entropy generation due to heat transfer irreversibility, while

$$N_{s,f} = Br\left[\left(\frac{dW}{d\xi}\right)^2 + \mathrm{MW}^2\right],$$

accounts for entropy generation due to viscous dissipation and magnetic field effects. The Bejan number (Be) is defined as the

ratio of thermal entropy generation to the total entropy generation and is given by

$$\mathrm{Be} = \frac{N_{s,h}}{N_{s,h} + N_{s,f}}, 0 \le \mathrm{Be} \le 1.$$

Physically, values of Be approaching unity indicate dominance of heat transfer irreversibility, whereas values close to zero imply that fluid friction and magnetic field effects dominate the entropy generation process.

Nusselt Number: The Nusselt number measures the effectiveness of convective heat transfer relative to conduction along the surface and is given by:

$$\mathrm{Nu} = -\frac{d\theta}{d\xi}\bigg|_{\text{wall}}.$$

At the bottom plate ($\xi = 0$):

$$\mathrm{Nu}_0 = -\frac{d\theta}{d\xi}\bigg|_{\xi=0}. \tag{14}$$

At the top plate ($\xi = 1$): From the boundary condition

$$\frac{d\theta}{d\xi}\bigg|_{\xi=1} = -\mathrm{Bi} \cdot \theta_1,$$

we obtain:

$$\mathrm{Nu}_1 = \mathrm{Bi} \cdot \theta_1. \tag{15}$$

Skin-Friction Coefficient: The skin-friction coefficient at the walls is proportional to the wall shear stress, and in dimensionless form it is given by:

$$C_f = \frac{dW}{d\xi}\bigg|_{\text{wall}}.$$

At the Lower Wall ($\xi = 0$):

$$C_{f0} = \frac{dW}{d\xi}\bigg|_{\xi=0}. \tag{16}$$

At the Upper Wall ($\xi = 1$):

$$C_{f1} = \frac{dW}{d\xi}\bigg|_{\xi=1}. \tag{17}$$

2.1 | Justification for Neglecting Thermal Radiation

In the present study, thermal radiation effects are neglected in the energy equation. This assumption is justified through an order of magnitude analysis comparing radiative and conductive heat transfer mechanisms. Using the Rosseland diffusion approximation, the radiative heat flux in the transverse direction can be expressed as

$$q_r \sim \frac{16\sigma T_m^3}{3\kappa}\frac{\Delta T}{L},$$

where σ is the Stefan–Boltzmann constant, T_m is a characteristic mean temperature, κ is the mean absorption coefficient, and L is the distance between the plates. The corresponding conductive heat flux is given by

$$q_c \sim k\frac{\Delta T}{L}.$$

The relative importance of thermal radiation to conduction is therefore measured by the radiation conduction parameter

$$Rd = \frac{q_r}{q_c} = \frac{16\sigma T_m^3}{3k\kappa}.$$

For moderate temperature differences and optically thick fluids, which are typical of liquid metals and electrically conducting fluids considered in MHD channel flows, the parameter $\mathrm{Rd} \ll 1$. Consequently, radiative heat transfer is negligible compared to conductive heat transfer, justifying its exclusion from the energy equation.

3 | Finite Difference Scheme

To solve the coupled nonlinear boundary value problem in steady-state as described in the dimensionless momentum and energy equations, we employ a finite difference discretization scheme. The spatial domain $0 \le \xi \le 1$ is divided into N_ξ uniform subintervals, with grid spacing $\Delta\eta = \frac{1}{N_\xi}$. The grid points are defined as $\xi_i = (i-1)\Delta\xi$, where $1 \le i \le N_\xi + 1$.

Let w_i and θ_i denote the numerical approximations of $w(\xi_i)$ and $\theta(\xi_i)$, respectively. The central difference schemes are used to approximate the second-order derivatives in the model equations as follows:

$$\frac{W_{i+1} - 2W_i + W_{i-1}}{(\Delta\xi)^2} - \left(\frac{1}{\mathrm{Da}} + M\right)W_i = A, \tag{18}$$

$$\frac{\theta_{i+1} - 2\theta_i + \theta_{i-1}}{(\Delta\xi)^2 \cdot \mathrm{Pr}} + \mathrm{Ec}\left(\frac{W_{i+1} - W_{i-1}}{2\Delta\xi}\right)^2 + \mathrm{EcMW}_i^2 + Q = 0, \tag{19}$$

where $A = \frac{1}{\nu U_0}\frac{dP}{dx}$ is a constant pressure gradient term.

At the upper plate ($\xi = 1$), the convective boundary condition is implemented using a second order backward difference:

$$\frac{\theta_{N_\xi+1} - \theta_{N_\xi}}{\Delta\xi} = -\mathrm{Bi}\ \theta_{N_\xi+1},$$

where Bi is the Biot number.

The finite difference scheme obeys the following boundary conditions:

$$W_1 = 0, \theta_1 = 1, \tag{20}$$

$$W_{N_\xi+1} = 0, \frac{\theta_{N_\xi+1} - \theta_{N_\xi}}{\Delta\xi} = -\mathrm{Bi} \cdot \theta_{N_\xi+1}. \tag{21}$$

3.1 | Numerical Solution Procedure

The coupled discretized momentum and energy equations are solved iteratively using the following procedure:

- Initialize the velocity W_i and temperature θ_i fields with initial guesses satisfying the boundary conditions.
- Update the velocity field W_i by solving the discretized momentum equation using the current temperature field.
- Update the temperature field θ_i by solving the discretized energy equation using the latest velocity field.
- Compute the maximum absolute changes in W_i and θ_i between successive iterations.
- Repeat steps 2–4 until the maximum change in both fields is less than a prescribed convergence tolerance, 10^{-6}.

This iterative procedure ensures that the coupling between the velocity and temperature fields is properly accounted for, yielding a converged steady-state solution.

4 | Results and Discussion

A grid independence study was performed by varying N_ξ from 50 to 200. Negligible changes in velocity and temperature were observed for $N_\xi \geq 150$, which was adopted for all simulations. Convergence was achieved when the maximum absolute change in both velocity and temperature between successive iterations was below 10^{-6}. To ensure realism, numerical computations are performed within parameter ranges relevant to practical MHD flow in porous channels. The Darcy number is taken as $0 < \mathrm{Da} < 1$, the magnetic interaction parameter as $0 \leq M \leq 20$, and the pressure gradient parameter as $0 < A \leq 2.1$. The Biot number varies within $0 \leq \mathrm{Bi} \leq 0.6$, while the Prandtl number is chosen in the range $5 < \mathrm{Pr} \leq 10$. The Eckert number is selected as $0.1 < \mathrm{Ec} \leq 2.6$ to account for viscous dissipation effects, and the internal heat generation parameter is varied within $0 \leq Q \leq 2.0$. The results in Figure 2 reveal that, increasing the Darcy number (Da) raises permeability, deepening velocity profiles and increasing temperatures due to improved heat retention. Entropy generation intensifies near the wall before decaying, reflecting higher irreversibility. These trends highlight the balance between thermal enhancement and entropy production, requiring an optimal Da. For the impermeable-wall limit ($\mathrm{Da} \to 0$), the numerical results reduce to those of classical MHD channel flow with stationary impermeable plates. The computed velocity and temperature profiles show excellent agreement with previously published results reported by Makinde [45] and Makinde and Chinyoka [46], thereby confirming the correctness of the numerical implementation in the Darcy limit.

The analysis in Figure 3 indicates that, as the magnetic parameter (M) increases, velocity decreases due to Lorentz forces slowing the flow. This observation, when compared with the results of Makinde and Azizi [5], Rashid et al., [26], Ngiangia and Orukari [47], Makinde [45], Makinde and Chinyoka [46] and Rotimi [48] agrees quantitatively. The results show that increasing the magnetic parameter from $M = 0$ to $M = 20$ reduces the entropy generation by 18% and reduces peak temperatures, especially near the walls, indicating improved thermodynamic efficiency and greater flow stability under stronger magnetic fields. These observations agree with results of Makinde and Azizi [5] and Mahian et al. [24].

Increasing the pressure constant (A) slows the fluid more sharply toward the channel center while raising temperatures, enhancing thermal energy. Entropy generation rises near the walls then decays across the channel, implying higher irreversibility with stronger pressure gradients, which can affect system performance as depicted in Figure 4.

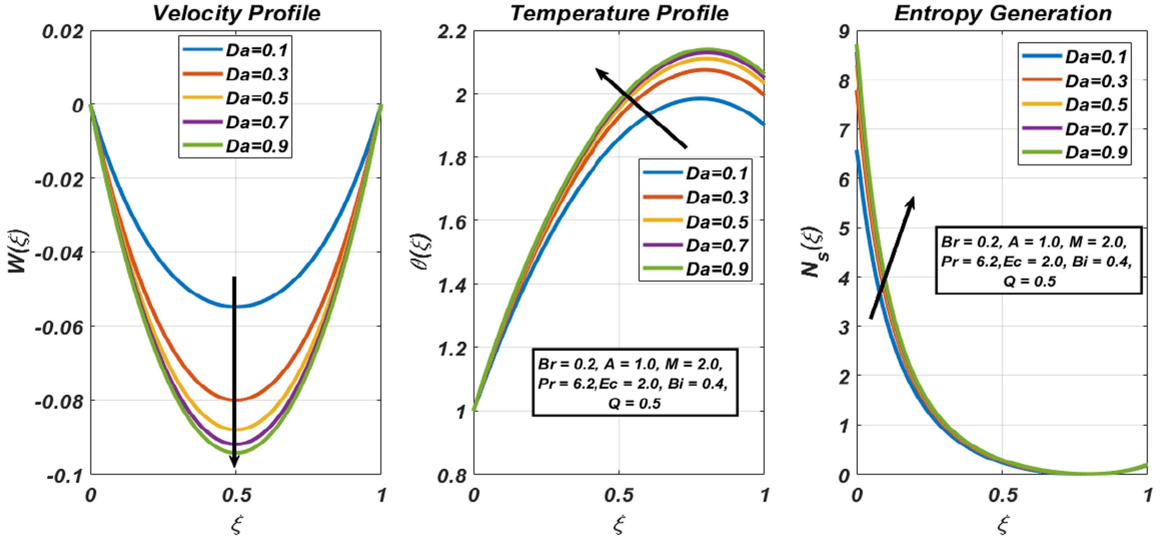

FIGURE 2 | Variation of Darcy number Da. [Color figure can be viewed at wileyonlinelibrary.com]

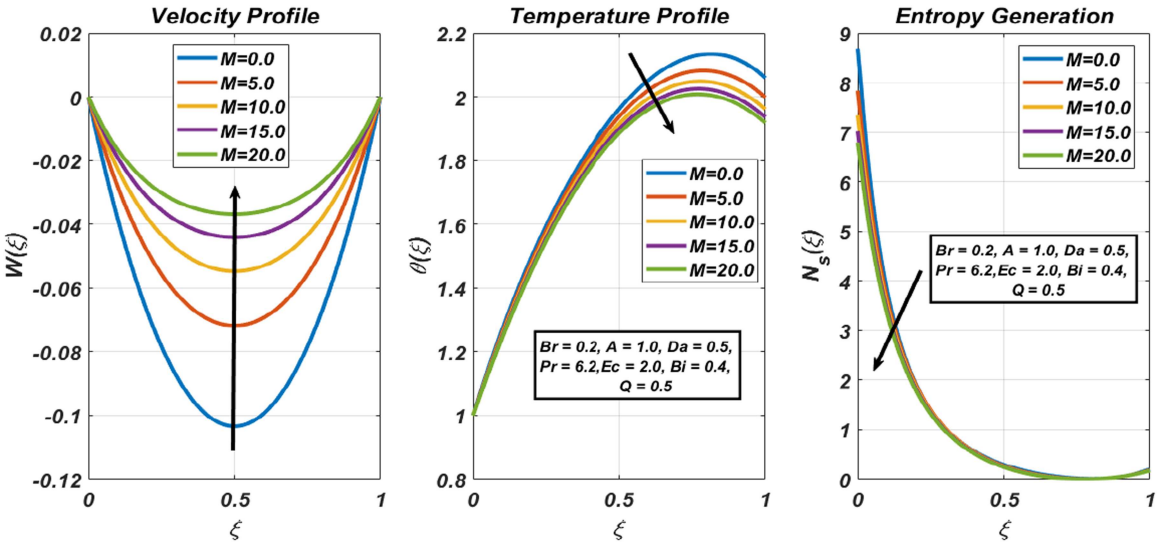

FIGURE 3 | Variation of magnetic parameter (M). [Color figure can be viewed at wileyonlinelibrary.com]

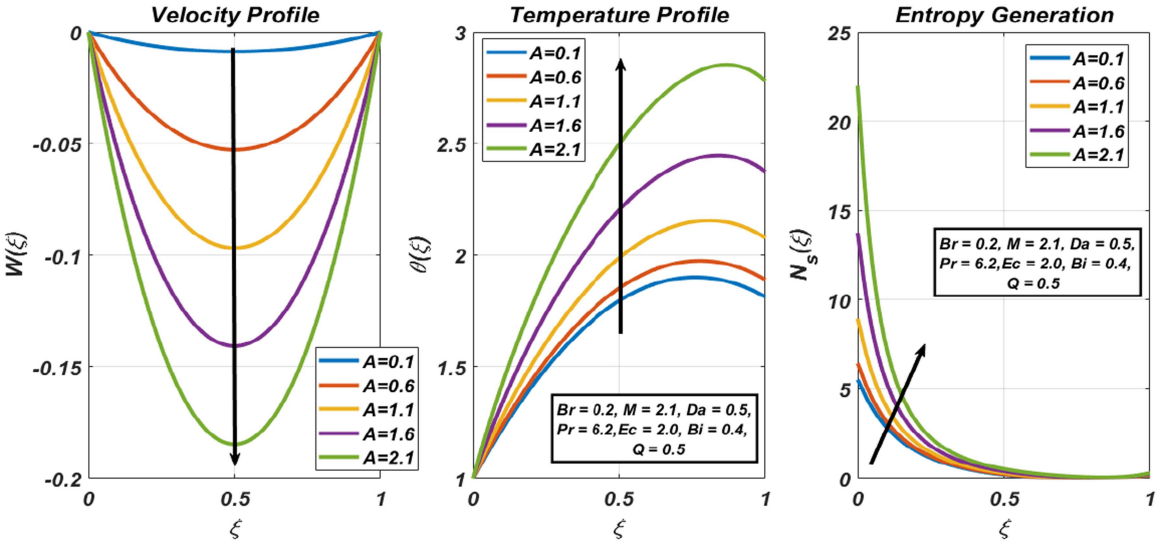

FIGURE 4 | Variation of the pressure constant (A). [Color figure can be viewed at wileyonlinelibrary.com]

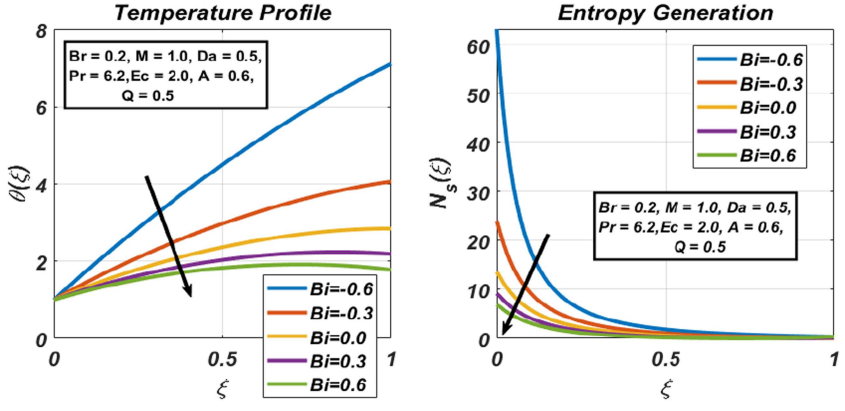

FIGURE 5 | Variation of Biot number (Bi). [Color figure can be viewed at wileyonlinelibrary.com]

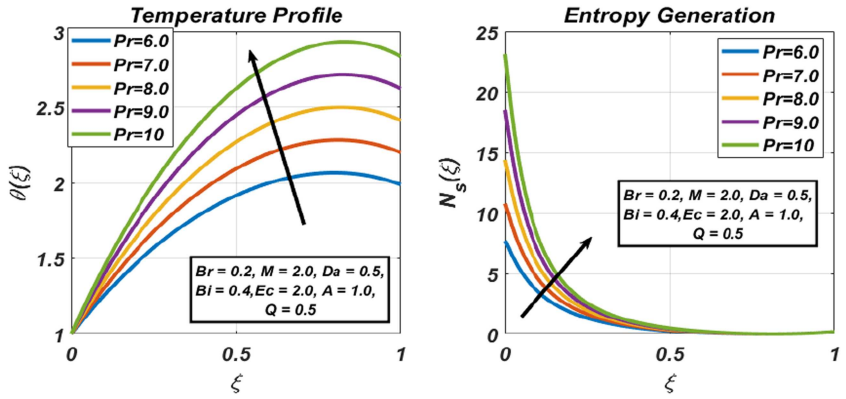

FIGURE 6 | Variation of Prandtl number (Pr). [Color figure can be viewed at wileyonlinelibrary.com]

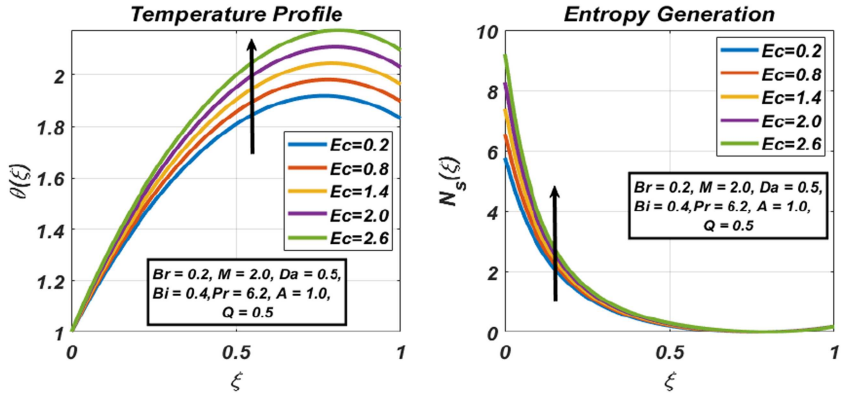

FIGURE 7 | Variation of Eckert number (Ec). [Color figure can be viewed at wileyonlinelibrary.com]

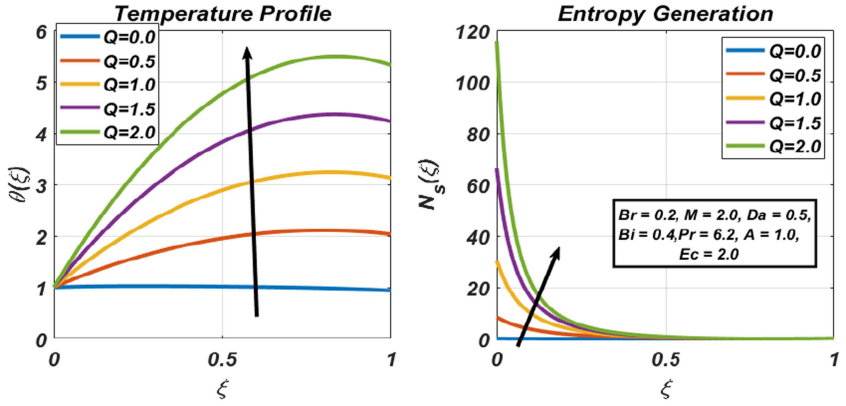

FIGURE 8 | Variation of the heat generation parameter (Q). [Color figure can be viewed at wileyonlinelibrary.com]

Moreover, the findings in Figure 5 proves that, higher Biot number (Bi) improves convective cooling, reducing fluid temperatures. This observations align perfectly with the results of Makinde and Chinyoka [46]. Also, the results reveal that, increasing the Biot number from Bi = 0 to Bi = 0.6 leads to a reduction of entropy generation of about 12%. This indicates that stronger magnetic fields and increased convective cooling at the upper plate effectively reduce thermodynamic irreversibilities. Consequently, enhanced surface heat transfer improves thermal efficiency, which is beneficial for cooling and MHD applications in porous media.

Increasing Prandtl number (Pr) results in higher and delayed temperature peaks, showing that high Pr implies that, fluids (such as water) retain more heat. Entropy generation is highest near the wall and drops inward, indicating that while heat retention is improved, there is a risk of higher thermal irreversibility near boundaries as shown in Figure 6.

Furthermore, the results in Figure 7 indicate that, greater Eckert number (Ec) raises temperatures through viscous dissipation of kinetic energy into heat. This results agrees with the findings of Makinde and Azizi [5] and Makinde [45]. Entropy generation intensifies near the inlet but converges downstream, showing the

TABLE 1 | Skin friction and Nusselt number results at varying M, Da, A, Ec, Q, and Bi.

M	Da	A	Ec	Q	Bi	$W''(0)$	$W''(1)$	$\theta'(0)$	$-\theta'(1)$
0.0	0.5	1.0	2.0	0.5	0.4	0.9915	0.9915	2.9412	0.8235
5.0	0.5	1.0	2.0	0.5	0.4	0.9774	0.9774	2.7955	0.7992
10.0	0.5	1.0	2.0	0.5	0.4	0.9681	0.9681	2.7063	0.7844
2.0	0.2	1.0	2.0	0.5	0.4	0.9774	0.9774	2.7043	0.7841
2.0	0.4	1.0	2.0	0.5	0.4	0.9836	0.9836	2.8376	0.8063
2.0	0.6	1.0	2.0	0.5	0.4	0.9860	0.9860	2.8993	0.8165
2.0	0.3	0.6	2.0	0.5	0.4	0.5888	0.5888	2.5036	0.7506
2.0	0.3	1.2	2.0	0.5	0.4	1.1776	1.1776	2.9799	0.8300
2.0	0.3	1.8	2.0	0.5	0.4	1.7664	1.7664	3.7737	0.9623
2.0	0.3	1.2	0.1	0.5	0.4	1.1776	1.1776	2.3766	0.7294
2.0	0.3	1.2	0.5	0.5	0.4	1.1776	1.1776	2.5036	0.7506
2.0	0.3	1.2	0.9	0.5	0.4	1.1776	1.1776	2.6306	0.7718
2.0	0.3	1.2	2.0	0.0	0.4	1.1776	1.1776	0.3493	0.3916
2.0	0.3	1.2	2.0	0.3	0.4	1.1776	1.1776	1.9277	0.6546
2.0	0.3	1.2	2.0	0.6	0.4	1.1776	1.1776	3.5060	0.9177
2.0	0.3	1.2	2.0	0.9	0.1	1.1776	1.1776	5.8894	0.3757
2.0	0.3	1.2	2.0	0.9	0.3	1.1776	1.1776	5.3114	0.9537
2.0	0.3	1.2	2.0	0.9	0.5	1.1776	1.1776	4.8876	1.3775

need to optimize Ec for balanced heat utilization and reduced irreversibility. This is similar to the findings of Mahian et al. [24].

More interestingly, the analysis in Figure 8 shows that, increasing the heat generation parameter (Q) results in higher fluid temperatures and elevated entropy generation, particularly near the inlet, reflecting greater irreversibility. This highlights the importance of optimizing Q for effective thermal management and minimal energy loss. These results align with the findings of Mahian et al. [24].

In a nutshell, the analysis is also focused on the Nusselt number, which quantifies the convective heat transfer rate at the channel walls, and the skin-friction coefficient, which measures the wall shear stress. The results in Table 1 reveal that, the Nusselt number at the bottom plate Nu_0 corresponds to $\theta'(0)$, while at the top plate Nu_1 is related to $-\theta'(1)$. These results reveal that higher Biot numbers and Eckert numbers generally enhance the Nusselt numbers, signifying stronger convective heat transfer. Meanwhile, the skin-friction coefficients at the lower and upper walls, given by $C_{f0} = W''(0)$ and $C_{f1} = W''(1)$ respectively, reflect how the momentum boundary layer reacts to variations in M, Da, and A. A higher magnetic field parameter M typically reduces the skin friction due to the Lorentz damping effect, while changes in permeability (Da) and pressure gradient (A) shift the wall shear stresses accordingly. Overall, tuning these parameters offers a means to control both momentum and thermal transport performance in a porous channel with convective heat transfer and magnetic field effects.

5 | Conclusion

The parametric analysis highlights the interplay of permeability, magnetic forces, pressure gradients, convective cooling, fluid properties, viscous dissipation, and internal heat generation on the velocity, temperature, and entropy generation in a porous channel. Key findings include:

- Higher Darcy numbers and heat generation rates increase thermal buildup and entropy generation, while stronger magnetic fields and higher Biot numbers reduce temperature, stabilize flow, and improve thermodynamic efficiency.
- Increased Prandtl numbers enhance thermal retention but can elevate entropy near the boundaries; higher Eckert numbers convert more mechanical energy into heat, increasing irreversibility.
- The Nusselt number increases with Biot and Eckert numbers, improving heat transfer, whereas skin friction decreases with stronger magnetic fields and varies with permeability and pressure gradient.

From an engineering perspective, these results provide practical guidance:

- Select moderate Darcy and Eckert numbers to balance flow resistance and thermal utilization.
- Apply appropriate magnetic field strengths to regulate velocity, reduce entropy generation, and control flow stability.
- Increase Biot numbers where enhanced convective cooling is desired.
- Optimize heat generation and match fluid Prandtl numbers to system requirements to minimize entropy production and improve energy efficiency.

These findings can inform the design and operation of porous channel thermal systems in applications such as heat

exchangers, magnetic cooling devices, and MHD systems, enabling improved thermal management with minimal irreversibility.

Nomenclature

Symbol	Description (SI Unit)
u	velocity in the x-direction [m/s]
T	temperature [K]
P	pressure [Pa]
ρ	fluid density [$\mathrm{kg/m^3}$]
μ	dynamic viscosity [Pa·s]
$\nu = \mu/\rho$	kinematic viscosity [$\mathrm{m^2/s}$]
$\alpha = k/(\rho c_p)$	thermal diffusivity [$\mathrm{m^2/s}$]
c_p	specific heat at constant pressure [J/(kg·K)]
k	thermal conductivity [W/(m·K)]
K	permeability of porous medium [$\mathrm{m^2}$]
σ	electrical conductivity [S/m]
B_0	magnetic field strength [T]
Q_0	internal heat generation [$\mathrm{W/m^3}$]
L	distance between plates [m]
$T_w(0)$	wall temperature at lower plate [K]
T_a	ambient temperature [K]
L_c	convective heat transfer coefficient [$\mathrm{W/(m^2 \cdot K)}$]
$\xi = y/L$	dimensionless transverse coordinate
$W = u/U_0$	dimensionless velocity
$A = \frac{1}{\nu U_0}\frac{dP}{dx}$	dimensionless pressure gradient term
$\theta = \frac{T - T_a}{T_w - T_a}$	dimensionless temperature
N_s	entropy generation number
$\mathrm{Be} = \frac{N_{s,h}}{N_{s,h} + N_{s,f}}$	Bejan number
$\mathrm{Pr} = \frac{\nu}{\alpha}$	Prandtl number
$\mathrm{Ec} = \frac{U_0^2}{c_p(T_w - T_a)}$	Eckert number
$M = \frac{\sigma B_0^2 L^2}{\rho \nu}$	magnetic parameter (Hartmann number squared)
$\mathrm{Da} = \frac{K}{L^2}$	Darcy number
$Q = \frac{Q_0 L^2}{k(T_w - T_a)}$	heat generation parameter
$\mathrm{Bi} = \frac{L_c L}{k}$	Biot number
$\mathrm{Br} = \frac{\mu U_0^2}{k(T_w - T_a)}$	Brinkman number
Nu	Nusselt number (convective to conductive heat transfer ratio)
$\mathrm{Nu}_0 = -\frac{d\theta}{d\xi}\Big\|_{\xi=0}$	Nusselt number at the lower wall
$\mathrm{Nu}_1 = \mathrm{Bi} \cdot \theta_1$	Nusselt number at the upper wall
C_f	skin-friction coefficient (dimensionless wall shear stress)
$C_{f0} = \frac{dW}{d\xi}\Big\|_{\xi=0}$	skin-friction coefficient at the lower wall
$C_{f1} = \frac{dW}{d\xi}\Big\|_{\xi=1}$	skin-friction coefficient at the upper wall

Author Contributions

All authors contributed equally to the conceptualization, methodology, analysis, and writing of this manuscript.

Acknowledgments

The authors extend their appreciation to the Deanship of Research and Graduate Studies at King Khalid University for funding this work through Large Research Project under grant number RGP.2/246/46.

Conflicts of Interest

The authors declare no conflicts of interest.

Data Availability Statement

All data generated/analyzed in this study can be obtained from the corresponding author upon justified request. The data are not publicly available due to privacy or ethical restrictions.

References

1. A. Bejan and J. Kestin, "Entropy Generation Through Heat and Fluid Flow," *Journal of Applied Mechanics* 50, no. 2 (1983): 475.

2. F. M. White and J. Majdalani, Viscous fluid flow (McGraw-Hill, 2006), Vol. 3, 433–434.

3. A. Z. Şahin, "Entropy Generation in Turbulent Liquid Flow Through a Smooth Duct Subjected to Constant Wall Temperature," *International Journal of Heat and Mass Transfer* 43, no. 8 (2000): 1469–1478.

4. S. Mahmud and R. A. Fraser, "Thermodynamic Analysis of Flow and Heat Transfer Inside Channel With Two Parallel Plates," *Exergy, an International Journal* 2, no. 3 (2002): 140–146.

5. O. D. Makinde, "Mhd Mixed-Convection Interaction With Thermal Radiation and nth Order Chemical Reaction Past a Vertical Porous Plate Embedded in a Porous Medium," *Chemical Engineering Communications* 198, no. 4 (2010): 590–608.

6. O. D. Makinde, "Entropy Analysis for Mhd Boundary Layer Flow and Heat Transfer over a Flat Plate With a Convective Surface Boundary Condition," *International journal of Exergy* 10, no. 2 (2012): 142–154.

7. O. Kigodi, M. H. Mkwizu, A. X. Matofali, et al., "Numerical Investigation of Entropy Generation in Unsteady MHD Generalized Couette Flow With Convective Cooling," *Communication in Mathematical Modeling and Applications* 4, no. 3 (2019): 95–111.

8. M. H. Mkwizu and O. D. Makinde, "Entropy Generation in a Variable Viscosity Channel Flow of Nanofluids With Convective Cooling," *Comptes Rendus Mecanique* 343, no. 1 (2015): 38–56.

9. O. J. Kigodi and N. H. Masasila, "Thermodynamic Irreversibility of Steady Viscous Couette Flow With Convective Cooling and Temperature-Dependent Viscosity," *Heat Transfer* (2025), https://doi.org/10.1002/htj.70087.

10. O. D. Makinde and A. Aziz, "MHD Mixed Convection From a Vertical Plate Embedded in a Porous Medium With a Convective Boundary Condition," *International Journal of Thermal Sciences* 49, no. 9 (2010): 1813–1820.

11. M. Faisal, F. Mabood, I. A. Badruddin, M. Aiyaz, and F. M. Butt, "Entropic Behavior With Activation Energy in the Dynamics of Hyperbolic-Tangent Mixed-Convective Nanomaterial Due to a Vertical Slendering Surface," *Multidiscipline Modeling in Materials and Structures* 20, no. 2 (2024): 341–362.

12. M. K. Mondal, N. Biswas, N. K. Manna, and A. J. Chamkha, "Enhanced Magnetohydrodynamic Thermal Convection in a Partially Driven Cavity Packed With a Nanofluid-Saturated Porous Medium," *Mathematical Methods in the Applied Sciences* (2021).

13. M. Faisal, I. Ahmad, and M. A. Awan, "Analysis of Entropy Generation and Activation Energy in Unsteady Double Diffusive Flow Over a Stretching Cylinder," *Heat Transfer* 53, no. 2 (2024): 646–665.

14. M. Faisal, I. Ahmad, and A. Rashid, "Entropic Behavior in Bidirectional Flow of CeO2-ZnO/Water Hybrid Nanofluid With

Prescribed Surface Temperature/Heat Flux Aspects," *Multidiscipline Modeling in Materials and Structures* 20, no. 1 (2024): 40–58.

15. A. Miles and R. Bessaïh, "Heat Transfer and Entropy Generation Analysis of Three-Dimensional Nanofluids Flow in a Cylindrical Annulus Filled With Porous Media," *International Communications in Heat and Mass Transfer* 124 (2021): 105240.

16. M. I. Khan, M. U. Hafeez, T. Hayat, M. I. Khan, and A. Alsaedi, "Magneto Rotating Flow of Hybrid Nanofluid With Entropy Generation," *Computer Methods and Programs in Biomedicine* 183 (2020): 105093.

17. S. Sindhu and B. J. Gireesha, "Entropy Generation Analysis of Hybrid Nanofluid in a Microchannel With Slip Flow, Convective Boundary and Nonlinear Heat Flux," *International Journal of Numerical Methods for Heat & Fluid Flow* 31, no. 1 (2021): 53–74.

18. M. M. Nandeppanavar, K. Vajravelu, M. S. Abel, and M. N. Siddalingappa, "Second Order Slip Flow and Heat Transfer Over a Stretching Sheet With Non-Linear Navier Boundary Condition," *International Journal of Thermal Sciences* 58 (2012): 143–150.

19. T. A. Alkanhal, M. Sheikholeslami, A. Arabkoohsar, et al., "Simulation of Convection Heat Transfer of Magnetic Nanoparticles Including Entropy Generation Using CVFEM," *International Journal of Heat and Mass Transfer* 136 (2019): 146–156.

20. R. D. Murugan, N. Sivakumar, N. Tarakaramu, H. Ahmad, and S. Askar, "Entropy Generation on MHD Motion of Hybrid Nanofluid With Porous Medium in Presence of Thermo-Radiation and Ohmic Viscous Dissipation," *Discover Applied Sciences* 6, no. 4 (2024): 199.

21. P. K. Kameswaran, M. Narayana, P. Sibanda, and G. Makanda, "on Radiation Effects on Hydromagnetic Newtonian Liquid Flow Due to An Exponential Stretching Sheet," *Boundary Value Problems* 2012 (2012): 1–16.

22. R. A. Mohamed, S. M. Abo-Dahab, A. M. Abd-Alla, and M. S. Soliman, " Magnetohydrodynamic Double-Diffusive Peristaltic Flow of Radiating Fourth-Grade Nanofluid Through a Porous Medium With Viscous Dissipation and Heat Generation/absorption," Scientific Reports 13, no. 1 (2023)13096. *Applied Mathematics and Computation*, 219(5), 2391–2403.

23. I. Mejri, A. Mahmoudi, M. A. Abbassi, and A. Omri, "Magnetic Field Effect on Entropy Generation in a Nanofluid-Filled Enclosure With Sinusoidal Heating on Both Side Walls," *Powder Technology* 266 (2014): 340–353.

24. O. Mahian, A. Kianifar, C. Kleinstreuer, et al., "A Review of Entropy Generation in Nanofluid Flow," *International Journal of Heat and Mass Transfer* 65 (2013): 514–532.

25. O. D. Makinde and A. Aziz, "MHD Mixed Convection From a Vertical Plate Embedded in a Porous Medium With a Convective Boundary Condition," *International Journal of Thermal Sciences* 49, no. 9 (2010): 1813–1820.

26. M. M. Rashidi, S. Abelman, and N. F. Mehr, "Entropy Generation in Steady MHD Flow Due to a Rotating Porous Disk in a Nanofluid," *International Journal of Heat and Mass transfer* 62 (2013): 515–525.

27. M. I. Khan, S. Ahmad Khan, T. Hayat, M. Faisal Javed, and M. Waqas, "Entropy Generation in Radiative Flow of Ree-Eyring Fluid Due to Due Rotating Disks," *International Journal of Numerical Methods for Heat & Fluid Flow* 30, no. 4 (2020): 1839–1865.

28. N. Biswas, D. K. Mandal, N. K. Manna, R. S. R. Gorla, and A. J. Chamkha, "Magnetohydrodynamic Thermal Characteristics of Water-Based Hybrid Nanofluid-Filled Non-Darcian Porous Wavy Enclosure: Effect of Undulation," *International Journal of Numerical Methods for Heat & Fluid Flow* 32, no. 5 (2022): 1742–1777.

29. M. H. Mkwizu, A. X. Matofali, and N. Ainea, "Entropy Generation in a Variable Viscosity Transient Generalized Couette Flow of Nanofluids With Navier Slip and Convective Cooling," *International Journal of Advances in Applied Mathematics and Mechanics* 5, no. 4 (2018): 20–29.

30. I. S. Mfinanga and A. Iddi, "Effect of Magnetic Field on the Wall Permeable Channel Flow With Convective Cooling," *International Journal of Advances in Scientific Research and Engineering* 338 (2020): 116768.

31. G. Mandal and D. Pal, "Mixed Convective-Quadratic Radiative Mos 2-SiO 2/H 2 O Hybrid Nanofluid Flow Over An Exponentially Shrinking Permeable Riga Surface With Slip Velocity and Convective Boundary Conditions: Entropy and Stability Analysis," *Numerical Heat Transfer, Part A: Applications* 85, no. 14 (2024): 2315–2340.

32. A. Rauf, S. A. Shehzad, A. Khalid, T. Mushtaq, and I. Ali, "Bödewadt Flow of Thermally Radiative Hybrid Nanofluid Under the Implication of Horizontal Magnetic Field," *Numerical Heat Transfer, Part A: Applications* (2024): 1–19.

33. K. Sakkaravarthi and P. B. A. Reddy, "Entropy Optimization of MHD Hybrid Nanofluid Flow Through a Curved Stretching Sheet With Thermal Radiation and Heat Generation: Semi-Analytical and Numerical Simulations," *Proceedings of the Institution of Mechanical Engineers, Part E: Journal of Process Mechanical Engineering* 237, no. 2 (2023): 138–148.

34. M. Kiamari, N. Sadooghi, and M. Sedighi Jafari, "Relativistic Magnetohydrodynamics of a Spinful and Vortical Fluid: Entropy Current Analysis," *Physical Review D* 109, no. 3 (2024): 036024.

35. K. Abuasbeh, B. Ahmed, A. U. K. Niazi, and M. Awadalla, "Entropy Generation for MHD Peristaltic Transport of Non-Newtonian Fluid in a Horizontal Symmetric Divergent Channel," *Symmetry* 15, no. 2 (2023): 359.

36. M. A. Abbas, Y. Q. Bai, M. M. Rashidi, and M. M. Bhatti, "Application of Drug Delivery in Magnetohydrodynamics Peristaltic Blood Flow of Nanofluid in a Non-Uniform Channel," *Journal of Mechanics in Medicine and Biology* 16, no. 04 (2016): 1650052.

37. P. V. Subrahmanyam, G. Kathyayani, G. V. Ramudu, and K. Venkatadri, "The Stagnation Point Flow of the Mhd Casson Polymeric Nanofluid Flows Toward a Wavy Circular Cylinder Saturated With a Porous Medium under Convective Nield Conditions and Thermal Radiation," *East European Journal of Physics* no. 3 (2025): 168–179.

38. S. Fazuruddin, S. Arigela, A. Shobha, V. R. Rajeswari, and K. Venkatadri, "Influence of Lorentz Force and Arrhenius Activation Energy on Radiative Bio-Convective Micropolar Nanofluid Flow With Melting Heat Transfer Over a Stretching Surface," *East European Journal of Physics* no. 3 (2025): 194–208.

39. C. Venkata Lakshmi, K. Swetha Sri, and K. Venkatadri, "Computational Analysis of Magnetized Heat Transfer in a Non-Darcy Porous Enclosure Using Ternary Hybrid Nanofluid and Finite Volume MAC Method," *International Journal of Modern Physics B* (2025): 2550217.

40. C. V. Lakshmi, A. Aravapalli, K. Venkatadri, O. A. Bég, and V. R. Prasad, "Impact of Joule Heating and Hydro-Magnetic Effects on Mixed Convection in Porous Cavity Using Lattice Boltzmann Method," *East European Journal of Physics* no. 2 (2025): 383–397.

41. H. Kim, K. Thirumalaisamy, and K. Venkatadri, "Computational Analysis of Magnetohydrodynamic Buoyancy-Driven Flow and Thermal Transmission Within a Circular Dome-Shaped Porous Enclosure Using Finite Difference Scheme," *International Journal of Numerical Methods for Heat & Fluid Flow* 35, no. 5 (2025): 1642–1679.

42. C. Venkata Lakshmi, K. S. Sri, K. Venkatadri, and O. Anwar Beg, "Simulation of Partial Magnetic Field Effects on Cu-TiO2-Water Hybrid Nanofluid Natural Convection Flow in a Darcy-Brinkman-Forchheimer Porous Media Enclosure With a MAC-FVM Combined Scheme," *International Journal of Computational Materials Science and Engineering* (2025).

43. G. Venkata Ramudu, G. Kathyayani, and K. Venkatadri, "Magnetohydrodynamic Double-Diffusive Convection of Casson Fluid in an

Irregular Pentagonal Cavity With Radiation and Chemical Reaction Effects," *Computational Mathematics and Modeling* (2025): 1–24.

44. O. D. Makinde and A. S. Eegunjobi, "Effects of Convective Heating on Entropy Generation Rate in a Channel With Permeable Walls," *Entropy* 15, no. 5 (2013): 1652–1671.

45. O. D. Makinde, "on Mhd Boundary-Layer Flow and Mass Transfer Past a Vertical Plate in a Porous Medium With Constant Heat Flux," *International Journal of Numerical Methods for Heat & Fluid Flow* 19, no. 3/4 (2009): 546–554.

46. O. D. Makinde and T. Chinyoka, "Numerical Investigation of Transient Heat Transfer to Hydromagnetic Channel Flow With Radiative Heat and Convective Cooling," *Communications in Nonlinear Science and Numerical Simulation* 15, no. 12 (2010): 3919–3930.

47. A. T. Ngiangia and M. A. Orukari, "MHD Couette-Poiseuille Flow in a Porous Medium," *Global Journal of Pure and Applied Mathematics* 9, no. 2 (2013): 169–181.

48. H. A. Rotimi and G. J. Abiodun, "Thermal Stability of a Reactive Hydromagnetic Poiseuille Fluid Flow Through a Channel," *American Journal of Applied Mathematics* 2, no. 1 (2014): 14–20.